Lithium-Gold Reference Electrode for Potential Stability During *In Situ* Electron Microscopy Studies of Lithium-Ion Batteries

Journal of The Electrochemical Society, 2020 **167** 110515

Lithium-Gold Reference Electrode for Potential Stability During *In Situ* Electron Microscopy Studies of Lithium-Ion Batteries

Jing Hou, Robin Girod, Nikolaos Nianias, Tzu-Hsien Shen, Jialiang Fan, and Vasiliki Tileli[z]

Institute of Materials, École Polytechnique Fédérale de Lausanne, CH-1015 Lausanne, Switzerland

Electrochemical liquid-phase transmission electron microscopy (TEM) is showing excellent promise in fundamental studies of energy-related processes including lithium-ion battery (LIB) cycling. A key requirement to accurately interpret the measurements and acquire quantitative information is the implementation of a reliable reference electrode. Quasi-reference electrodes (QRE) remain commonly used due to microfabrication constraints of the electrochemical cell, however, they typically yield dramatic potential drifts making the electrochemical results inconclusive. Here, we present a method of producing a stable and readily interpretable lithium-gold alloy micro-reference electrode, which exhibits a reference potential of 0.1 V vs Li/Li^+. We first examine the feasibility of electrochemically alloying a pristine gold electrode, patterned on a chip for *in situ* TEM, using a benchtop setup, and investigate various sources to support the lithiation. We confirm the presence of the Li-Au alloy using chronopotentiometry (CP) and open circuit voltage (OCV) measurements, and by scanning electron microscopy (SEM), electron energy loss spectroscopy (EELS) and high-resolution (HR) TEM. Finally, we apply this methodology *in situ* and use $LiFePO_4$ as a model cathode material to demonstrate the merit of the Li-Au alloy reference electrode for obtaining reproducible cyclic voltammetry (CV) measurements on a liquid cell microelectrode system.

 [DOI: 10.1149/1945-7111/ab9eea]

Manuscript submitted April 25, 2020; revised manuscript received June 4, 2020. Published July 7, 2020.

Electrochemical transmission electron microscopy (TEM) in liquids enables real-time observation of material transformations during electrochemical processes.[1–4] Pertinent to lithium-ion battery (LIB) cycling, early work involved electrochemical nucleation, growth and dendrite formation.[5,6] More recently, electrochemical TEM studies in liquids were used to determine phase maps of $LiFePO_4$ cathode transformations during cyclic voltammetry (CV)[4] and to monitor elemental dissolution of $Li_{1+x}(Ni_{0.6}Co_{0.2}Mn_{0.2})_{1-x}O_2$ cathodes during CV and galvanostatic charge/discharge analysis.[7] Despite the progress and the insights gained thus far, monitoring real-time positive or negative electrode degradation mechanisms and interpreting their behavior under electron beam irradiation is hindered by the stability of the reference electrode. The reliability of a system for analyzing electrochemical-induced transformations in single electrodes in batteries is determined by having a reference electrode that preserves a constant and well-defined potential over time. In bulk cells, metallic lithium is usually considered as the material of choice, although lithium alloys and Li-intercalation compounds exhibiting a two-phase structure have also been investigated.[8]

For *in situ* TEM studies, the range of usable electrode materials is constrained by the scale of the cell and by the micromechanical fabrication procedure of the components of the cell. As a result, commercially available electrodes are currently limited to Pt, Au, Ni, Cu, or C/Pt. The use of these materials as quasi-reference electrodes (QRE) presents two important shortcomings. First, QREs may exhibit critical potential shifts over time, or may be modified during operation. This is particularly the case with *in situ* TEM where the influence of the electron beam on the electrolyte and the electrodes themselves remains poorly controlled. Second, limited literature is available on the use of these QREs for the study of LIB electrode materials, making it difficult to readily interpret and compare electrochemical results obtained in the TEM with bulk studies.

A way to circumvent these issues was recently presented by different groups. For example, Lim et al. used a metallic lithium foil counter/reference electrode that was placed in an external container and was ionically connected to the microcell chamber via the electrolyte tube.[9] Such design was successfully used to measure potentials similar to values obtained in coin cells, during correlated cycling of $LiFePO_4$ particles and compositional mapping of the (de) lithiation state by situ scanning transmission X-ray microscopy (STXM). Using a similar setup, Unocic et al. were able to characterize the dynamics of solid electrolyte interphase (SEI) formation and evolution on graphite by *in situ* TEM.[10] In both cases, the designs present limitations associated with the remote location of the counter/reference electrode with regard to the working electrode. This inevitably leads to an increased ohmic drop across the electrodes.

The challenge of implementing a stable micro-reference electrode in a battery is not, however, exclusive to the *in situ* microscopy field. There is a growing body of literature on reference electrodes in electrochemical impedance spectroscopy (EIS) investigations of LIBs where a Li reference electrode is electrochemically deposited or alloyed with metallic wires. In such experiments, a micro-sized reference electrode is indeed crucial to mitigate disruptions in the electrical field between symmetrical working and counter electrodes. Zhou et al. used electrodeposited lithium on a copper wire, however, depending on the plating parameters, the properties and stability of the plated film were impeded by the continuous SEI formation and dissolution of lithium ions into the electrolyte.[11] Recently, Solchenbach et al. used a gold wire that thermodynamically resulted in an alloy when lithiated.[12] Due to the greater chemical stability of Li-Au alloys and to a small exposed area with regard to the total alloyed volume, their reference electrode was stable for several weeks and exhibited a reference potential indicative of a Li_xAu ($0 < x < 1.2$) alloy.[13]

Stemming from the interest in Li_xAu as an anode material, previous *in situ* TEM studies focused on the cycling behavior and structural evolution of gold films during lithiation and delithiation.[14,15] While these reports establish the feasibility of electrochemically alloying lithium and gold in an *in situ* TEM apparatus, their methodologies need to be adapted and mild alloying conditions need to be defined in order to achieve a structurally undamaged and stable reference electrode for electrochemical electron microscopy studies.

Here, we report on the alloying of lithium with a gold micro-electrode thin film patterned on the electrochemical chip and on its performance as a stable reference electrode for liquid-phase TEM investigations of LIBs. We first establish the feasibility of this procedure *ex situ* and outside of the TEM holder and investigate various sources such as metallic lithium, $LiFePO_4$ delithiation, and reduction of Li salt containing electrolyte, to support the lithiation of

[z]E-mail: vasiliki.tileli@epfl.ch

the gold micro-electrodes using chronopotentiometry (CP). We investigate the morphological modifications induced by this step with scanning electron microscopy (SEM) and TEM and confirm the formation of a Li-Au alloy using electron energy-loss spectroscopy (EELS) and high-resolution (HR)TEM. We then show that this methodology can be applied directly in an *in situ* TEM holder to obtain a Li_xAu reference electrode stable over hours whose potential can be directly related to bulk values from the literature. We cycle $LiFePO_4$ as a model cathode and show that reproducible and coherent measurements can be performed outside and *in situ* in the TEM with limited effects of the electron beam on the electrochemical signal, thereby demonstrating the merit of our reference electrode for future *in situ* TEM investigations of LIB electrode materials. Finally, the chemical stability of the electrolyte during the full process is confirmed by nuclear magnetic resonance (NMR) spectroscopy.

Experimental

Electrochemical micro-chips for* in situ *TEM measurements.— The chips have been designed and manufactured in-house to fit in a TEM liquid-electrochemistry holder (Hummingbird Scientific, Lacey, WA, USA) and create a microfluidic cell as previously described.[16,17] They feature three thin film electrodes patterned in a co-planar configuration (Fig. 1), one of them running through a SiN_x electron-transparent window to provide observable areas in the TEM. The configuration used in this study features two platinum electrodes ($E_{Pt,1}$, on the window, and $E_{Pt,2}$, the counter one) and one gold electrode in the middle (E_{Au}) intended to be lithiated and used as the reference electrode. The patterned electrodes are partially isolated from the electrolyte by a passivation layer (SiO_2) deposited on top, except for the regions of the electron transparent window and of the contacts with the holder pins. By doing so, the electrochemical reaction sites can be optimized within the viewing region. The non-passivated (electrochemically active) surface areas of the three electrodes are 0.1553 mm^2 for E_{Au}, 0.11 mm^2 for $E_{Pt,1}$, and 0.4974 mm^2 for $E_{Pt,2}$.

Site-specific deposition of $LiFePO_4$ (LFP) particles.—For LFP deposition on $E_{Pt,1}$ or $E_{Pt,2}$, the particles were dispersed in a solution of 10 mg ml^{-1} polyvinylidene fluoride (PVDF, Kynar HSV 900) dissolved in 1-methyl-2-pyrrolidinone (NMP, 99.5%, AcroSeal) that act as a binder for the particles, in a weight ratio of 1:6. The suspension was pipetted with a capillary (Narishige GD-C 1, Tokyo, Japan) pulled by a Narishige puller (Narishige PC-10, Tokyo, Japan), and then was dropcast on the selected electrode using a micromanipulator (Narishige MMO-4 hydraulic micromanipulator combined with a mechanical coarse manipulator) in ambient atmosphere. The prepared chip was heated at 60 °C for 12 h to remove NMP in the Ar-filled glovebox.

Reference electrode preparation in open cell configuration.— Open cell setup conducted in the glovebox was used for practical reasons and in order to allow for various materials to be tested as lithium sources for alloying. In particular, galvanostatic lithiation of gold thin films supported by metallic lithium or by decomposition of lithium hexafluorophosphate salt ($LiPF_6$)-containing electrolyte has been reported in the literature.[13,18,19] In addition to those known lithium sources, we also investigated the feasibility of using the charge (i.e. oxidation at the counter electrode) of LFP particles to support the lithiation current, in an attempt to avoid electrolyte decomposition.

When using metallic lithium, experiments were conducted in a beaker as presented in Fig. 1a, with the chip and a lithium plate clamped separately as the working and counter/reference electrodes respectively and both immersed in a standard electrolyte containing 1 M $LiPF_6$ in a 3:7 weight ratio of ethylene carbonate (EC) and ethyl methyl carbonate (EMC) (LP57, w-w $<$ 20 ppm H_2O, BASF SE, Germany). Lithiation from LP57 reduction or LFP particles delithiation was carried out by mounting the chip on a flexible flat cable/flexible printed circuit connector (FFC/FPC, Molex, 52207 series), allowing for connection with all three electrodes outside of the holder while leaving the non-passivated area exposed (Figs. 1b, 1c). A 2 μl droplet of electrolyte was cast on the electrodes within the membrane region. The gold electrode was lithiated by applying a current between the counter electrode ($E_{Pt,2}$ pristine, or LFP deposited on $E_{Pt,2}$) and the gold electrode. Nominal C rates were derived from the applied current and a calculated initial gold weight estimated from the gold electrode surface area (0.1553 mm^2), using the bulk value of the density of gold (ρ_{Au} = 19.3 g cm^{-3}). The chip was rinsed with dimethyl carbonate (DMC, anhydrous, ⩾99% Sigma-Aldrich) after lithiation and was dried at 60 °C in the glovebox for post mortem characterization with electron microscopy, includingSEM, STEM and EELS.

Chemical stability assessment after lithiation.—Once the electroplating of lithium was finished (or after the *in situ* experiments), the electrolyte was collected in an NMR tube within the Ar glovebox and mixed with dimethyl sulfoxide-d6 (DMSO-d6, 99.9 atom % D, anhydrous Sigma-Aldrich). The solution was then subjected to analysis with liquid NMR spectroscopy (AV NEO-400, Bruker, 400 MHz).

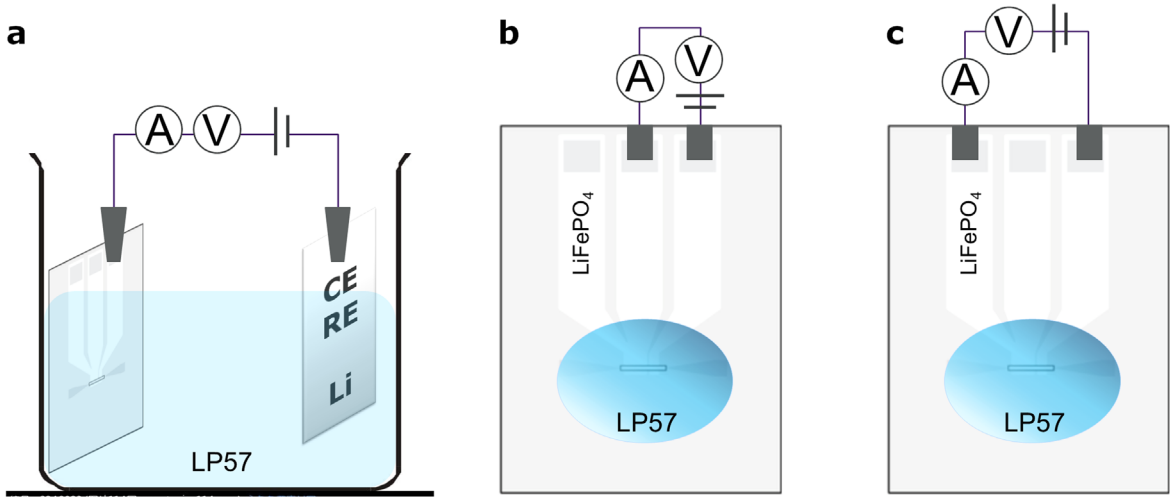

Figure 1. (a) The glass cell setup for gold lithiation by metallic lithium. Lithium was clamped as counter and reference electrode, while the gold, working electrode on the chip was lithiated by applying negative current. (b)–(c) The open cell setup for gold lithiation either from the electrolyte (b) or $LiFePO_4$ particles (c). $LiFePO_4$ particles were dropcast on the electrode that has the largest conductive surface.

Reference electrode assessment in liquid cell.—Prior to experiments in the holder, the electrochemical chip was air-plasma treated at 100 W for 2.5 min. After assembling the cell with a bottom chip (spacer, 1 μm) in ambient atmosphere, the holder was stored under vacuum for 1–2 h for degassing before transferring it inside an Ar-filled glovebox, so that the remaining air and moisture were removed from the assembled cell through the open microfluidic tube. Ar was then passed with a syringe through the liquid cell to remove possible air/moisture residues. The electrolyte (LP57) was introduced into the liquid chamber by the microfluidic tubes under the Ar atmosphere until a stable potential reading was achieved on the three electrodes.

Lithiated gold reference electrodes from LFP particles delithiation were prepared in the liquid cell by applying a current of 500 nA for 3 h between the LFP loaded counter electrode ($E_{Pt,2}$) and the gold electrode, while the third electrode ($E_{Pt,1}$), also loaded with LFP, was used as the effective reference electrode. The electrolyte was continuously flowed through the liquid cell with the help of a pumping system at a flow rate of 5 μl min^{-1}. Open circuit voltage measurement for 30 min was conducted after finishing the lithiation. For CVs of LFP, the connections were swapped to use the lithiated gold as the reference electrode, and $E_{Pt,1}$ was cycled against $E_{Pt,2}$ at 20 mV s^{-1} between 1.5 V and 5.5 V vs Li_xAu for five cycles. All the described electrochemical measurements were carried out in the glovebox. After sealing the fluidic tubes, the liquid cell was transferred to the TEM. Measurements were repeated for comparison.

Electron microscopy.—Morphology analysis was performed in a Zeiss Merlin SEM. Electronic structure and composition studies were performed by HRTEM (Talos 200 kV, ThermoFisher Scientific, USA) and EELS (Titan Themis 200 kV,ThermoFisher Scientific, USA). The *in situ* TEM was performed on aTEM operated at 200 kV (JEOL 2200FS, Japan).

Results and Discussion

Benchtop galvanostatic lithiation of gold reference electrode from various sources.—As a first step, galvanostatic lithiation of gold thin film reference electrodes patterned on the electrochemical chips was investigated in open cell. Fig. 2a shows the cell potential curves during gold lithiation supported by the oxidation of metallic lithium (at a nominal 32.67 C rate, 10 min, solid green curve), of LFP (3.27 C, 1 h, dotted red curve), and of the electrolyte (3.27 C, 1 h, dashed blue curve). Note that the open cell setup for lithiation from metallic lithium, LP57, or LFP is different, as described in the experimental part (and illustrated in Fig. 1) so that the potential differences are measured either between the gold electrode and lithium counter electrode (case of lithiation from metallic lithium) or between the gold electrode and another platinum electrode patterned on the chip either deposited with LFP particles or left pristine (case of LP57 reduction). In all three cases, a distinct first potential plateau can be observed (around 0.2 V vs Li/Li$^+$ in the metallic lithium experiment within the glass beaker, Fig. 2a, solid green curve, coherent with values reported for gold lithiation and Au-Li phase transformation and around −6 V for the other experiments on the chip).[12] A second plateau appears at −6.2 V in the LP57 case. In comparison, during lithiation from metallic lithium, the first plateau remains stable until the end of the experiment, while during lithiation from LFP, the cell voltage after the first plateau decreases slowly until the experiment is stopped. When LP57 is used as the lithiation medium, a clear potential drop at −6.2 V is observed at the beginning of the experiment before stabilizing at the first plateau, while the potential curve during lithiation from LFP does not exhibit any similar initial dip and stabilizes within 10 min of the experiment.

The coherent potential curves observed against Li/Li$^+$ during lithiation from metallic lithium show that the setup used for this experiment allows lithium ions to transfer from the counter electrode to the gold electrode efficiently. On the other hand, the large cell voltage recorded during lithiation from LP57 could indicate the decomposition of the electrolyte, with high oxidative potential required at the counter electrode in order to support the lithiation current. LFP nanoparticles used for the last experiment are likely to delithiate in the first minutes of the experiment, causing the small potential shoulder observed at −5.8 V (Fig. 2a—dotted red curve) and the discrepancies with the lithiation experiment from LP57. It is likely that the amount of lithium available from LFP is not enough to sustain the complete lithiation of the gold electrode and supplementary Li ions from the electrolyte become necessary over time.

Top-down and cross-sectional SEM images of the lithiated gold electrodes are depicted in Figs. 2b–2i. Compared to a pristine gold electrode surface (Fig. 2b), 300–500 nm diameter grains can be observed on the three lithiated electrode surfaces. Bulky extrusions of several microns are exclusively seen from the surface lithiated with metallic lithium with higher current. In the cross-sectional images, an inhomogeneous lithiation front within the gold electrode can be observed in all cases, with discrepancies in the depth of penetration between the methods. Differences in the surface layer morphology and thickness can also be observed, with the electrodes lithiated from LFP and LP57 exhibiting a thin ∼200 nm surface layer while the electrode lithiated from metallic lithium has a 1–2 μm layer clearly visible on top of the gold film.

These discrepancies between the methods could arise from the different rates used to lithiate the gold electrodes. Additionally, the protruding surface features are likely related to overcharging and subsequent lithium deposition, as the nominal C rates used were relatively high and were maintained beyond the specific capacity of the most Li-rich phase (Li_3Au, 408 mAh g^{-1}). It is noted that the rates used in this study were dictated by the setup. Reasons remain unclear, but when low current was applied to the cells (typically when inferior to 100 nA), the potential did not stabilize for the duration of the experiment, and no lithiation was observed. Finally, cell voltage plateaus during lithiation using metallic lithium or LP57 were stable well beyond the overcharge state. We hypothesize that this behavior arises from the lithiation of the silicon substrate which takes place around 0.1 V vs Li/Li$^+$, as the back of the chip was also connected by the clamp, as well as from possible diffusion of lithium under the passivation layer.[20]

Based on these results, gold electrode lithiation can be performed directly on the electrochemical TEM chips and the lithium source can be adjusted between metallic lithium or LP57. While deposited LFP seemingly does not provide enough lithium for lithiation of the gold electrode, obtaining lithium-depleted particles at the counter electrode can nevertheless provide an interesting anode material for *in situ* studies of high-potential cathodes such as Ni–Co–Mn layered oxides.[21]

Benchtop evaluation of lithiated gold stability.—To evaluate the stability of the lithiated gold electrode, we performed OCV measurements following an open cell lithiation at 100 nA for 3 h with LFP deposited on the counter electrode, Fig. 3. After the lithiation, the gold electrode potential ramps up to an initial relatively stable region at ∼−3.3 V vs $LiFePO_4$ within 40 min. Subsequently, a second plateau around −3 V appears at the 200 min mark and remains for the next 6 h, until the end of the measurement. Considering an LFP potential at 3.42 V vs Li/Li$^+$, the two observed regions would correspond to potentials of ∼0.1 V vs Li/Li$^+$ and ∼0.4 V vs Li/Li$^+$, matching well with gold delithiation plateaus previously reported in the literature and indicating a final Li_xAu alloy with $0 < x < 1$.[13,21,22]

We attribute the good stability of the second plateau to the diffusion of lithium under the passivation layer during galvanostatic lithiation. Since this area is not directly exposed to the electrolyte during the OCV, it would provide a lithium reserve which prevents lithium depletion in the non-passivated area, therefore mitigating possible SEI formation and side reactions with the electrolyte.

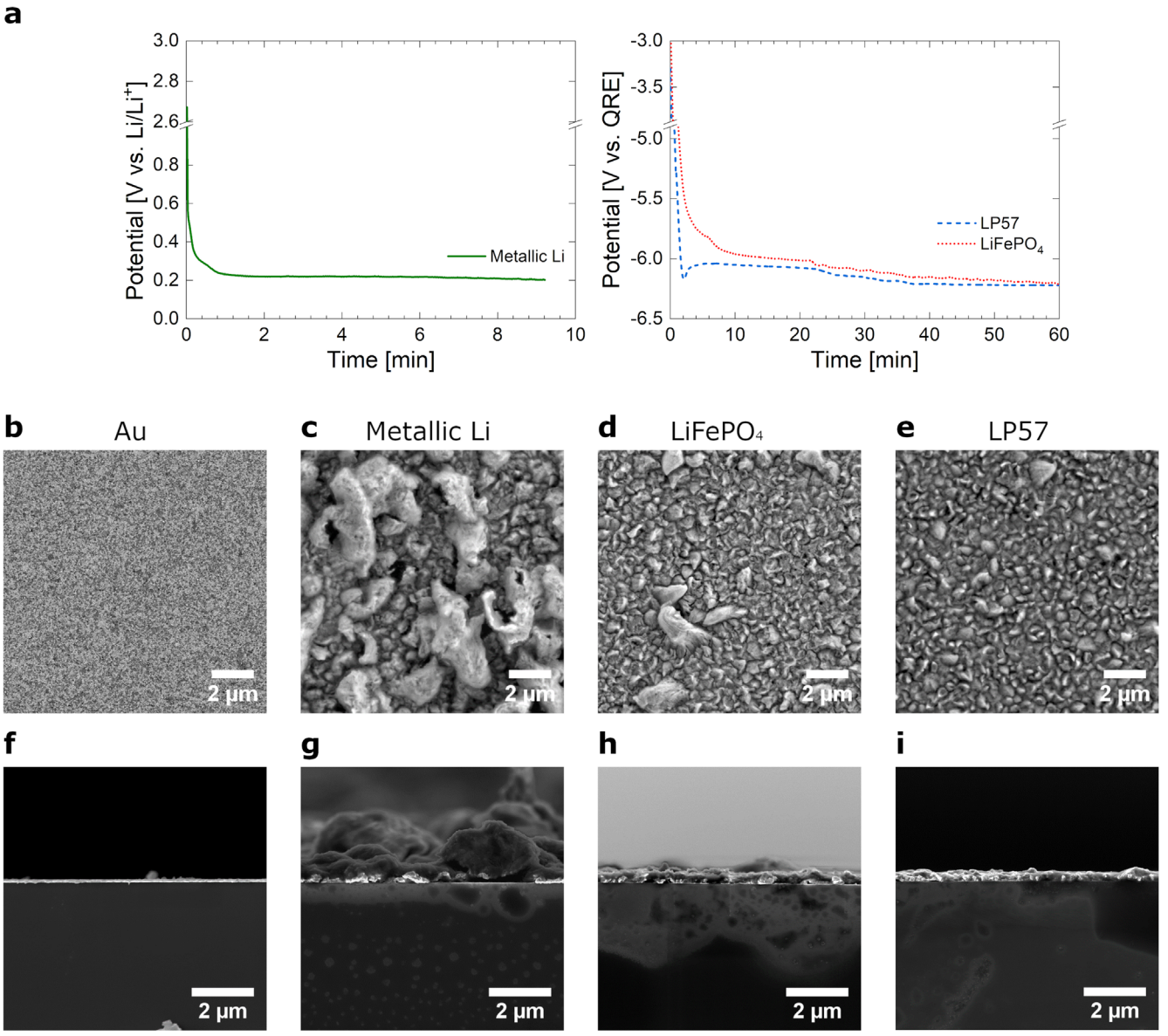

Figure 2. (a) Comparison of potential evolution of lithiated gold during galvanostatic lithiation from metallic lithium oxidation (solid green curve, vs Li/Li^+) at a 32.67 C rate (2 μA), from reduction of LP57 (dashed blue curve, QRE is Pt) and from $LiFePO_4$ particles oxidation (dotted red curve, QRE is LFP) both at a 3.27 C rate (200 nA). Top-view (b)–(e) and cross-sectional (f)–(i) SEM images of the pure Au electrode and the lithiated gold electrodes from metallic lithium, $LiFePO_4$, and LP57.

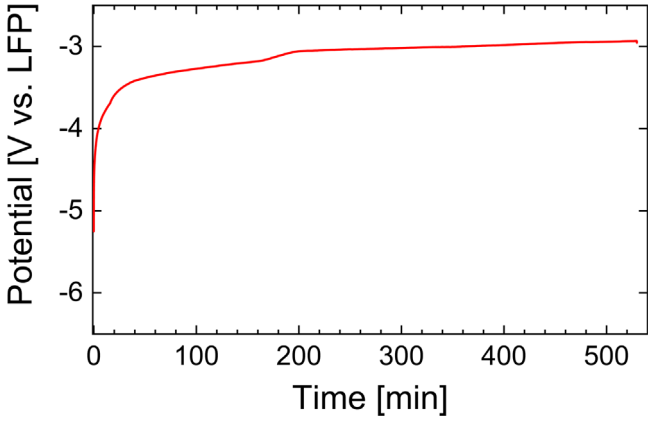

Figure 3. Open circuit voltage between lithiated gold electrode and delithiated LFP after 3 h of galvanostatic lithiation at 100 nA in the open cell.

Characterization of lithiated electrode.—To further confirm that Li is inserted in the structure, we performed TEM structural and chemical analysis. Fig. 4a shows an EEL spectrum acquired at the edge of a previously lithiated gold electrode, with the peak at 55 eV unambiguously confirming the presence of Li. STEM images of the gold electrode before and after lithiation are shown in Figs. 4b–4c. After lithiation, the structure becomes less dense and exhibits a porous structure that is consistent with previous studies on the fabrication of nanoporous metals by electrochemical alloying and de-alloying with lithium.[23,24] Finally, HRTEM micrographs of the pristine and lithiated gold electrodes were compared in order to acquire information on phase changes in the structure. The fast Fourier transform (FFT) of HRTEM image taken from the pristine electrode in Fig. 4d, shows cubic packed gold crystal structure. In contrast, the lithiated Au particles exhibit a crystalline pattern that matches well with the [0–1 2] zone axis of tetragonal $AuLiO_2$ alloys, Fig. 4e. The oxidation likely results from the transfer of the lithiated chip outside the glovebox for the *ex situ* analysis.

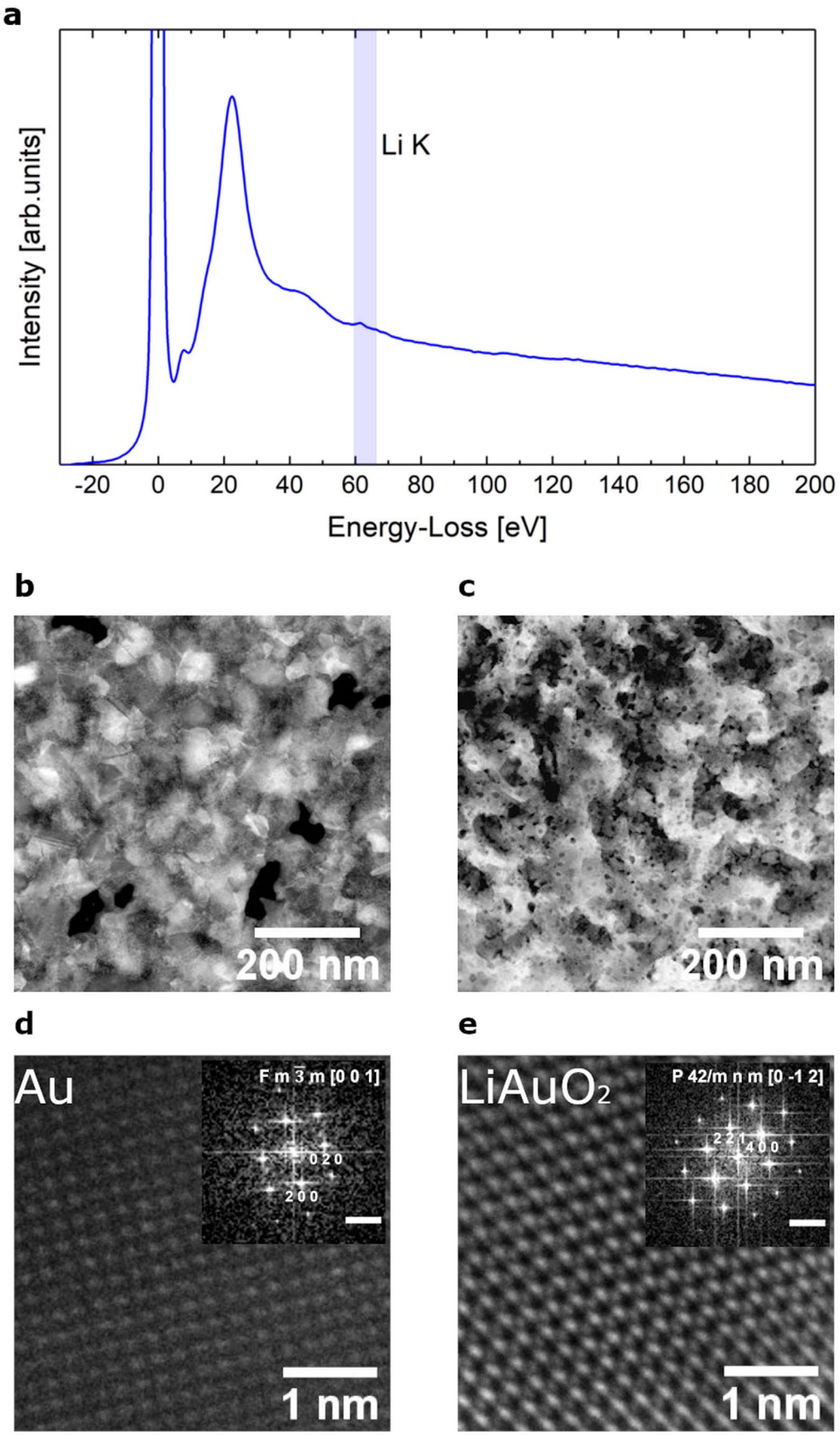

Figure 4. (a) Low-loss EEL spectrum of lithiated gold. (b)–(c) STEM images of bare and lithiated gold electrode. (d)–(e) HRTEM micrographs of the pristine gold electrode and of the lithiated gold respectively. The insets are the corresponding FFTs with the scale bar of 5 nm^{-1}.

Galvanostatic lithiation of gold reference electrode in liquid cell.—Having confirmed the feasibility of fabricating a Li_xAu microelectrode patterned on a chip, we examine its electrochemical performance for *in situ* experiments. A liquid cell was assembled in the *in situ* TEM holder, with LFP deposited on both platinum electrodes. The reference electrode was lithiated inside the glovebox by applying a 500 nA current between the counter electrode ($E_{Pt,2}$) and the gold electrode for 3 h under a 5 μl min^{-1} electrolyte flow rate. The cell voltage during the galvanostatic lithiation and the following 30 min OCV is presented in Fig. 5a. A plateau at −5.5 V was observed, with a decrease to −6 V after 130 min. While the cell voltage does not show as well-defined plateaus as during the open cell experiments, the subsequent OCV indicates a lithiated gold reference electrode potential of −3.3 V vs LFP, coherent with the previous measurements.

We note that lithiation attempts were successful only when a current above a certain threshold was applied. That is, for currents lower than 500 nA applied in the liquid cell, the gold electrode potential would quickly return to the pristine gold potential regardless of the duration of the lithiation. Furthermore, maintaining an electrolyte flow was necessary to avoid complete electrolysis of the electrolyte as the non-passivated surface area of the gold electrode used in this study is relatively large.

Electrochemical evaluation of lithiated gold as reference in liquid cell.—To demonstrate the merit of our reference electrode for *in situ* measurements, we then used LFP particles deposited on the chip's working electrode ($E_{Pt,1}$) as a model cathode material. Fig. 5b shows three CV profiles recorded against the pre-lithiated gold reference electrode, inside the glovebox and in the TEM with and without electron beam exposure. Each measurement exhibits the classical CV shape with well-defined oxidation and reduction peaks, without the dramatic effects of the electron beam previously reported.[14] Furthermore, each measurement was well reproducible over 5 cycles. The half-wave potentials $E_{1/2}$ are measured around 3.3 V, again demonstrating that the reference electrode exhibits a potential coherent with lithiated gold, about 0.1 V vs Li/Li^+.[25,26] A 50 mV shift is observed between the measurements in the glovebox and the one in the TEM, possibly indicating that the former was performed before complete stabilization of the reference potential. The further shift observed between measurements without and with electron beam irradiation is due to the significant decrease in the anodic peak in the latter. Despite a relatively low electron dose rate (42.6 $e^- nm^{-2} s^{-1}$), it is assumed that this decrease is associated with possible narrowing of the working potential window of the electrolyte due to increased beam-induced radicals and subsequent electrolyte degradation causing reduced ability for lithium transport.[27,28] This is further supported by the oxidative peak appearing at 5.1 V vs Li_xAu under irradiation. It is also interesting to note that the peak-to-peak distance is significantly reduced inside the TEM, indicating reduced ohmic losses. This could be associated with an increase in the liquid layer thickness due to the membrane bulging in the microscope.[4]

Chemical stability of the system.—In addition to the air-sensitive nature of lithium-ion battery experiments, the methodology to acquire a stable lithiated reference electrode requires overcharging of the lithium source which brings in the risk of electrolyte decomposition and adds complexity to the experimental setup for the subsequent electrochemical measurements. Therefore, we used nuclear magnetic resonance (NMR) spectroscopy of the liquid electrolyte to verify the chemical stability of our system after the electrochemical processing for reference electrode preparation. Test solutions were taken after the open cell lithiation of the reference electrode as well as after the *in situ* experiments. It is noted that despite the small volume of liquid electrolyte, sampling was possible. We compared these results with fresh and ambient-air-oxidized electrolyte solutions for reference, as depicted in Fig. 6. According to previous studies, the oxidation of $LiPF_6$ in LP57 mainly follows the route expressed in reactions 1 to 3.[29–32] Therefore, possible degradation of the electrolyte would be detected by the oxidized by-products such as PO_4^{3-}, PO_3F^{2-} and $PO_2F_2^-$, as shown in the air-exposed electrolyte NMR results. However, after open cell lithiation experiments with the constant volume of electrolyte or after lithiation conducted in the liquid cell with continuous flow of electrolyte, we confirm that the liquid electrolyte remains unaffected without evidence of considerable degradation of oxidative by-products and can therefore be readily used for the subsequent *in situ* electrochemical analysis.

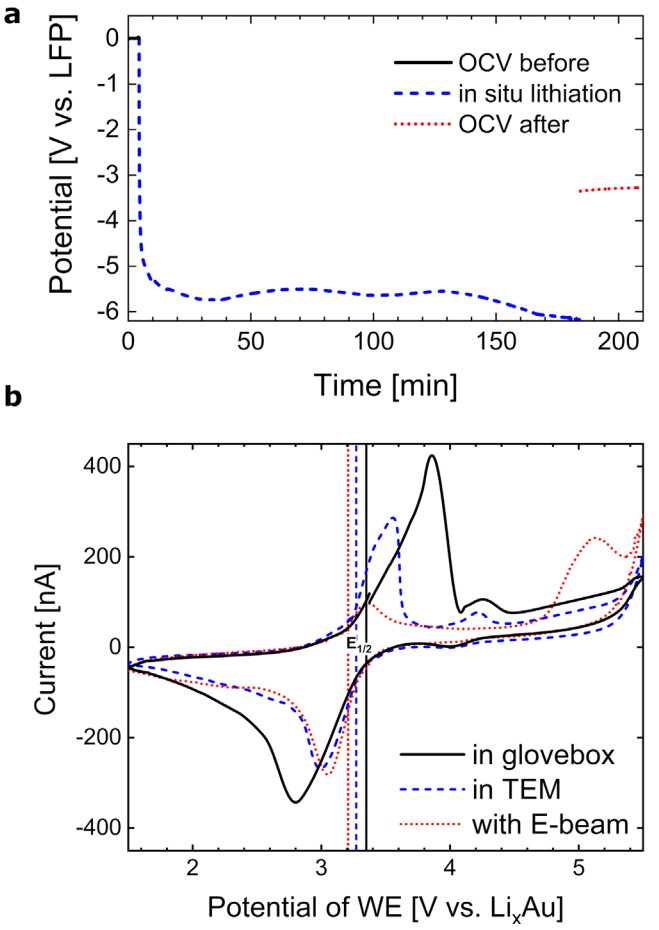

Figure 5. (a) Gold electrode lithiation with $LiFePO_4$ as the lithium source in liquid cell using CP by applying a constant current of 500 nA between the LFP counter electrode and gold electrode for 3 h followed by 30 min OCV. Dashed blue curve indicates the potential difference evolution between the lithiated gold electrode and the delithiated LFP loaded as lithium source on the counter electrode. Solid black and dotted red curves represent the OCV between them before and after lithiation respectively. (b) Cyclic voltammetry of LFP with delithiated LFP as counter electrode and lithiated gold as the reference electrode from 1.5 V to 5.5 V at 20 mV s^{-1} within the liquid cell holder in the glovebox (solid black curve), in the TEM with electron beam off (dashed blue curve) and on (dotted red curve). Electron dose rate was 42.6 $e^- nm^{-2} s^{-1}$.

$$PF_6^- + H_2O \leftrightharpoons POF_3 + 2HF + F^- \quad [1]$$

$$POF_3 + H_2O \leftrightharpoons PO_2F_2^- + HF + H^+ \quad [2]$$

$$PO_2F_2^- + H_2O \leftrightharpoons PO_3F^{2-} + HF + H^+ \quad [3]$$

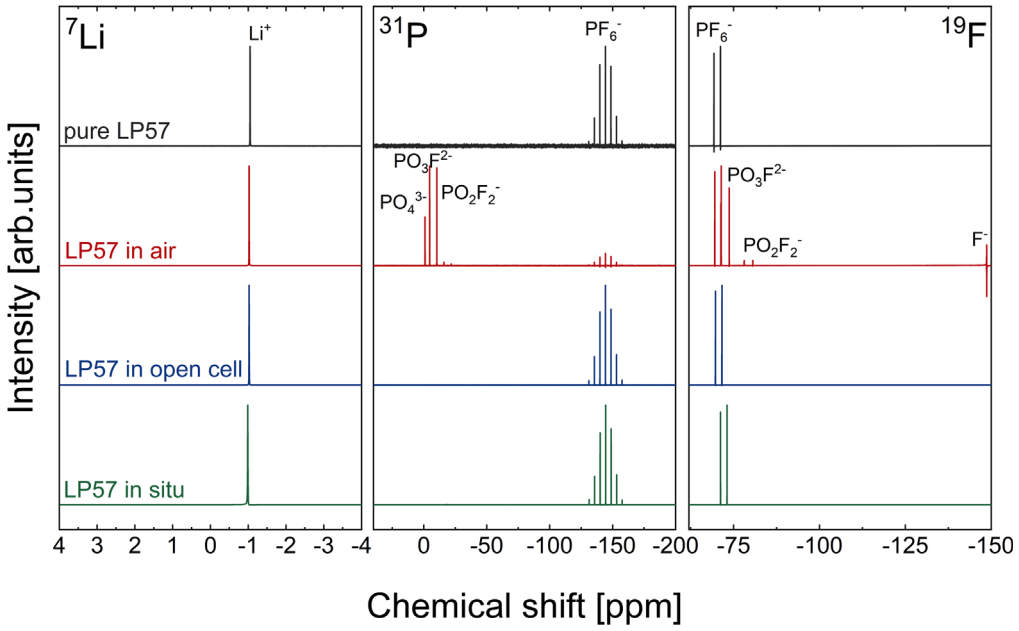

Figure 6. NMR spectra showing the ^{7}Li, ^{31}P and ^{19}F of the pure electrolyte LP57 (black), LP57 exposed in air for seven days (red), LP57 collected from the open cell experiments conducted in the glovebox (blue) and LP57 collected after the *in situ* experiments within the TEM liquid cell (green).

Conclusions

In summary, using a combination of *in situ* TEM and *ex situ* chemical characterization methods, we have demonstrated a practical way of fabricating a lithium-based reference electrode for *in situ* investigations of lithium-ion batteries. Stabilizing a reference electrode for microcell testing in confined space can be achieved on the bench and within an *in situ* TEM holder by applying a constant current for steady lithiation of a gold micro-electrode without damaging the substrate and by using various sources including metallic Li, Li salt electrolyte or $LiFePO_4$ particles. Furthermore, the system composed of the stable potential reference electrode of Li_xAu and the partially delithiated $LiFePO_4$ particles on the counter electrode can be beneficial for *in situ* studies of cathode materials. Therefore, such a micro-battery setup can be optimized into a reasonable and reproducible system for more adaptable and precise characterization of real-time observations using liquid-phase electrochemical TEM.

Acknowledgments

The research was partially supported by the BMW group (Munich, Germany) and the authors thank Dr. Filippo Maglia for useful discussions.

ORCID

Vasiliki Tileli https://orcid.org/0000-0002-0520-6900

References

1. F. Wu and N. Yao, *Nano Energy*, **11**, 196 (2015).
2. N. Hodnik, G. Dehm, and K. J. J. Mayrhofer, *Acc. Chem. Res.*, **49**, 2015 (2016).
3. Y. Yuan, K. Amine, J. Lu, and R. Shahbazian-Yassar, *Nat. Commun.*, **8**, 15806 (2017).
4. M. E. Holtz, Y. Yu, D. Gunceler, J. Gao, R. Sundararaman, K. A. Schwarz, T. A. Arias, H. D. Abruña, and D. A. Muller, *Nano Lett.*, **14**, 1453 (2014).
5. N. de Jonge and F. M. Ross, *Nat. Nanotechnol.*, **6**, 695 (2011).
6. F. M. Ross, *Science*, **350**, aaa9886 (2015).
7. J. Hou, A. Freiberg, T.-H. Shen, R. Girod, J. Gonthier, S.-J. Kim, F. Maglia, H. A. Gasteiger, and V. Tileli, *J. Phys.: Energy*, (2020).
8. F. La Mantia, C. D. Wessells, H. D. Deshazer, and Y. Cui, *Electrochem. Commun.*, **31**, 141 (2013).
9. J. Lim et al., *Science*, **353**, 566 (2016).
10. R. R. Unocic, X.-G. Sun, R. L. Sacci, L. A. Adamczyk, D. H. Alsem, S. Dai, N. J. Dudney, and K. L. More, *Microsc. Microanal.*, **20**, 1029 (2014).
11. J. Zhou and P. H. L. Notten, *J. Electrochem. Soc.*, **151**, A2173 (2004).
12. S. Solchenbach, D. Pritzl, E. J. Y. Kong, J. Landesfeind, and H. A. Gasteiger, *J. Electrochem. Soc.*, **163**, A2265 (2016).
13. P. Bach, M. Stratmann, I. Valencia-Jaime, A. H. Romero, and F. U. Renner, *Electrochim. Acta*, **164**, 81 (2015).
14. Z. Zeng, W.-I. Liang, Y.-H. Chu, and H. Zheng, *Faraday Discuss.*, **176**, 95 (2014).
15. A. J. Leenheer, K. L. Jungjohann, K. R. Zavadil, and C. T. Harris, *ACS Nano*, **10**, 5670 (2016).
16. E. Fahrenkrug, D. H. Alsem, N. Salmon, and S. Maldonado, *J. Electrochem. Soc.*, **164**, H358 (2017).
17. R. Girod, N. Nianias, and V. Tileli, *Microsc. Microanal.*, **25**, 1304 (2019).
18. P. Bach, I. Valencia-Jaime, U. Rütt, O. Gutowski, A. H. Romero, and F. U. Renner, *Chem. Mater.*, **28**, 2941 (2016).
19. K. Yan, Z. Lu, H. W. Lee, F. Xiong, P. C. Hsu, Y. Li, J. Zhao, S. Chu, and Y. Cui, *Nat. Energy*, **1**, 16010 (2016).
20. M. N. Obrovac and L. Christensen, *Electrochem. Solid-State Lett.*, **7**, A93 (2004).
21. H.-C. Liu, W.-H. Ho, C.-F. Li, and S.-K. Yen, *J. Electrochem. Soc.*, **155**, E178 (2008).
22. Y. Huang, H. Liu, L. Gong, Y. Hou, and Q. Li, *J. Power Sources*, **347**, 29 (2017).
23. P. Bai, J. Li, F. R. Brushett, and M. Z. Bazant, *Energy Environ. Sci.*, **9**, 3221 (2016).
24. K. Nishio, M. Yoshida, and H. Masuda, *ECS Electrochem. Lett.*, **2**, C43 (2013).
25. Y. Orikasa, T. Maeda, Y. Koyama, H. Murayama, K. Fukuda, H. Tanida, H. Arai, E. Matsubara, Y. Uchimoto, and Z. Ogumi, *Chem. Mater.*, **25**, 1032 (2013).
26. D. Y. W. Yu, C. Fietzek, W. Weydanz, K. Donoue, T. Inoue, H. Kurokawa, and S. Fujitani, *J. Electrochem. Soc.*, **154**, A253 (2007).
27. R. R. Unocic, R. L. Sacci, G. M. Brown, G. M. Veith, N. J. Dudney, K. L. More, F. S. Walden, D. S. Gardiner, J. Damiano, and D. P. Nackashi, *Microsc. Microanal.*, **20**, 452 (2014).
28. P. Abellan, T. J. Woehl, L. R. Parent, N. D. Browning, J. E. Evans, and I. Arsland, *Chem. Commun.*, **50**, 4873 (2014).
29. R. Younesi, G. M. Veith, P. Johansson, K. Edström, and T. Vegge, *Energy Environ. Sci.*, **8**, 1905 (2015).
30. E. Markevich et al., *Electrochem. Commun.*, **15**, 22 (2012).
31. M. Stich, M. Göttlinger, M. Kurniawan, U. Schmidt, and A. Bund, *J. Phys. Chem. C*, **122**, 8836 (2018).
32. R. Wagner, M. Korth, B. Streipert, J. Kasnatscheew, D. R. Gallus, S. Brox, M. Amereller, I. Cekic-Laskovic, and M. Winter, *ACS Appl. Mater. Interfaces*, **8**, 30871 (2016).